Review

International Journal of Modern Physics B
Vol. 27, No. 18 (2013) 1330011 (31 pages)

DOI: 10.1142/S0217979213300119

World Scientific
www.worldscientific.com

LONG-RANGE VAN DER WAALS INTERACTION

JIANMIN TAO*, JOHN P. PERDEW† and ADRIENN RUZSINSZKY†

Department of Physics and Engineering Physics,
Tulane University, New Orleans, LA 70118, USA
**jtao@tulane.edu*

Received 22 May 2013
Accepted 26 May 2013
Published 1 July 2013

Van der Waals interaction is an elusive many-body effect arising from instantaneous charge fluctuations. Fundamental understanding of this effect plays an important role in computational chemistry, physics and materials science. In this article, recent advances in the evaluation of van der Waals coefficients, in particular the higher-order ones, are reviewed.

Keywords: Long-range; van der Waals interaction; vdW coefficient; dynamic multipole polarizability; solid-sphere model; spherical shell.

PACS numbers: 31.15.ap, 31.15.E-, 34.20.-b

1. Introduction

In computer-aided design of electronic materials, devices and chemical or physical processes, accurate prediction of electronic properties plays a decisive role. Many correlated wavefunction-based *ab initio* methods, such as configuration interaction (CI),[1,2] many-body perturbation theory (MBPT),[3] coupled cluster,[4] quantum Monte Carlo,[5] or their combinations (e.g., CI+MBPT), are highly accurate, but computationally demanding. For large systems (e.g., systems that consist of more than 10^2 atoms), less accurate but improvable Kohn–Sham density functional theory (DFT),[6,7] noted for its high computational efficiency and useful accuracy, becomes a method of choice.

In Kohn–Sham DFT, everything is known, except for the exchange-correlation energy component, which has to be approximated as a functional of the electron density.[8,9] Due to the advent of reliable density functional approximations,[10–19] this theory has become a standard practice in modern electronic structure calculations. However, it is also known that these ordinary DFT methods often fail to describe

†Current address: Department of Physics, Temple University, Philadelphia, PA 19122, USA.

weakly bound systems, such as closed-shell atom and molecule pairs. In many cases, DFT predicts unbound or too-weak intermolecular pairs.[20] This failure greatly limits the applicability of DFT to a large class of weakly-bound systems such as atom and intermolecular pairs, liquids and molecular crystals. DFT can produce unusually large errors even for many normally-bonded molecules and solids.[21] A fundamental reason is that conventionally developed exchange-correlation functionals are unable to account for the long-range part of the van der Waals (vdW) interaction, while they may describe the short-range part well.[20] To overcome or reduce this difficulty, a dispersion correction, which can be developed separately, is usually added to DFT. This DFT+vdW approach can significantly improve the performance of ordinary DFT and has been widely used in electronic structure calculations.[22–27]

The vdW interaction is an important many-body effect, which arises from charge fluctuation of each density piece. It has the finite short-range or small-$\mathcal{R}$ expansion and the long-range or large-$\mathcal{R}$ limit, where $\mathcal{R}$ is the separation between centers of density pieces. Because many properties are related to the long-range part and because the short-range part can be well treated with first-principles calculations,[20] we will focus on the long-range part in this review article.

In the large separation ($\mathcal{R} \to \infty$) limit, the vdW interaction between any two density pieces can be exactly expressed as an infinite power series of the inverse $\mathcal{R}$,

$$E_{\rm vdW} = -\sum_{k=1} \frac{C_{2k}}{\mathcal{R}^{2k}} - \sum_{k=1} \frac{C_{2k+1}}{\mathcal{R}^{2k+1}} - \cdots , \tag{1}$$

where C_{2k}, with k being an integer, are the vdW coefficients. For specific systems, not all these terms appear in this expression simultaneously. For example, for a surface–surface interaction, C_2 is the leading-order coefficient,[28–30] which can be obtained from the dielectric response of each bulk solid, while C_3 is the leading-order coefficient for the particle-surface interaction. When the two interacting densities take the shape of spherical symmetry, the above expression may be simplified as:

$$E_{\rm vdW} = -C_6/\mathcal{R}^6 - C_8/\mathcal{R}^8 - C_{10}/\mathcal{R}^{10} - \cdots , \tag{2}$$

where C_6 describes the instantaneous dipole–dipole interaction, C_8 the dipole–quadrupole interaction and C_{10} the dipole–octupole and quadrupole–quadrupole interactions. This series is obviously divergent as the internuclear distance of two atoms tends to zero, where the true vdW (or dispersion) energy remains finite. To fix this problem, we can multiply each term, $C_{2k}R^{-2k}$, by a damping function $f(R)$, which suppresses the singularity at $R = 0$. Many damping functions have been proposed.[31–33] In the simulation of intermolecular potentials, the remaining but also the most difficult task is to find an accurate way to evaluate these vdW coefficients C_{2k}. According to second-order perturbation theory, vdW coefficients between two spherical densities can be calculated from the dynamic multipole polarizability $\alpha_l(iu)$ of each density piece, namely[34]:

$$C_{2k}^{\rm AB} = \frac{(2k-2)!}{2\pi} \sum_{l_1=1}^{k-2} \frac{1}{(2l_1)!(2l_2)!} \int_0^\infty du\ \alpha_{l_1}^{\rm A}(iu)\alpha_{l_2}^{\rm B}(iu)\,, \tag{3}$$

where $l_2 = k - l_1 - 1$ and $\alpha_l(iu)$ is the dynamic 2^l-pole polarizability of each density piece. iu is the imaginary frequency. Here l represents the vibrational mode of plasmon : $l = 1$ (dipole), $l = 2$ (quadrupole), $l = 3$ (octupole), etc.

The dynamic multipole polarizability defines the linear response of a system to a weak, time-dependent external electric field[35] oscillating at frequency ω. It may be calculated from perturbation theory with the sum-over-states expression,[36]

$$\alpha_l(iu) = \sum_{n=1}^{\infty} \frac{f_n^l}{(E_n - E_0)^2 + u^2}\,, \tag{4}$$

where E_n is the transition energy from the ground state Ψ_0 to the excited state Ψ_n. f_n^l is the oscillator strength proportional to the transition magnitude $|\langle\Psi_0|\Psi_n\rangle|^2$. It may be also evaluated from the density response function[37,38] defined by:

$$\chi_{nn}(\mathbf{r}, \mathbf{r}'; iu) = i \int_0^{\infty} d\tau e^{-u\tau} \langle\Psi|[\hat{n}(\mathbf{r}, \tau), \hat{n}(\mathbf{r}')]|\Psi\rangle\,. \tag{5}$$

In general, the response function $\chi_{nn}(\mathbf{r}, \mathbf{r}'; iu)$ is a highly nonlocal function in both space and time. It can be conveniently computed from time-dependent density functional theory (TDDFT)[39] linear response.[40] This theory, like the ground-state DFT, is formally exact, but the dynamic exchange-correlation potential or exchange-correlation kernel, defined as the functional derivative of the potential

$$f_{xc}(\mathbf{r}, \mathbf{r}'; t, t') = \frac{\delta v_{xc}([n]; \mathbf{r}, t)}{\delta n(\mathbf{r}', t')}\,, \tag{6}$$

must be approximated. Here $v_{xc}([n]; \mathbf{r}, t)$ is the time-dependent dynamic exchange-correlation potential.[41,42] The simplest construction is the adiabatic approximation,[43,44] in which the time-dependent exchange-correlation potential is calculated using the functional form of the ground-state potential, but with the ground-state density replaced by the instantaneous electron density. Due to the simplicity in theory and implementation, the adiabatic TDDFT has been most widely-used to study the time-dependent processes or excited states, including the long-range vdW interaction.[45,46] However, calculation of the response function for large systems becomes difficult even with efficient TDDFT.

This computational challenge may be addressed in two ways. The first (and also the easiest) is to use the intuitive "atom pairwise interaction picture",[47] which is perhaps the most popular approach due to its simplicity and reasonable accuracy. The atom pairwise interaction picture was originally proposed by Hamaker.[48] This picture works well for small or even some large molecules. However, we have recently found that it breaks down for nanosize or larger clusters. The second but more reliable way is to develop model dynamic polarizabilities.

Many models[49–63] have been proposed for the calculation of the vDW coefficients. Rapcewicz and Ashcroft[49] proposed a simple model for the dynamic dipole polarizability for an inhomogeneous system. It is based on the dynamic dipole polarizability of an extended uniform electron gas obtained from second-order perturbation theory, and generalization to inhomogeneous systems. Numerical tests

on rare-gas dimers show that this model can generate the leading-order coefficient C_6 in fairly good agreement with accurate reference values. Andersson, Langreth and Lundqvist[50] proposed a modification of the Rapcewicz–Ashcroft model by geometrically averaging the effective density. This modification leads to a good improvement of C_6 for rare-gas dimers, with a mean absolute relative error (MARE) of about 12%. In 2007, Becke and Johnson[55,56] proposed an exchange hole-based model, which extends their earlier calculation for the leading-order coefficient C_6 to higher-order coefficients C_8 and C_{10}. Numerical tests show that the model yields C_6 in excellent agreement (3%) with accurate reference values, without relying on any empirical fitting. However, the error of this model is quite large for C_8 and C_{10}, suggesting that the physics behind the model for C_6 is not entirely transferred to that for higher-order coefficients. This incorrect transfer may be related to the fact that all the inputs for C_6, C_8 and C_{10} are the same — the static dipole polarizability. Lima[54] extended an empirical model[53] for the dynamic dipole polarizability to the dynamic multipole polarizability, from which higher-order coefficients can be generated accurately. The inputs of this model are the static multipole polarizabilities. However, Lima's model contains several additional empirical parameters beyond those in the model dynamic dipole polarizability[53] and the number of empirical parameters increases with the order of vdW coefficients. The increase of empirical parameters makes the model physically untransparent.

Vydrov and Van Voorhis[59] proposed a model for the dynamic dipole polarizability. An appealing feature of this model is that the cutoff of plasmon vibrational contribution is smoothly carried out with a local band gap introduced by the authors. This model contains a fit parameter and produces C_6 with a MARE of about 10%. In recent years, Tkatchenko *et al.*[57,60] proposed several models to calculate C_6 for molecule pairs. Their starting point is the accurate reference values of C_6 for atom pairs. The basic idea is the atom pairwise interaction picture. Numerical tests on a considerable number of small molecules show that the method produces C_6 with an error of about 5%. The model has been used recently to study the properties of solids.[25,26]

Tao *et al.*[58] have proposed a simple model for the dynamic dipole polarizability. Numerical tests show that the model can accurately generate C_6 in excellent agreement (3%) with highly-accurate wavefunction-based many-body approach. Encouraged by the remarkable accuracy, the model was applied to study the dispersion correction to DFT for lattice constants and cohesive energies. It was shown that the unusually large error of DFT can be reduced to normal with the dispersion correction. In that work, we showed that the higher-order vdW interaction can be as large as 50% of the leading-order term. The significance of higher-order contributions may be reflected from a series of DFT dispersion corrections developed from Grimme's group,[22–24] among which the latest version contains the C_8 contribution. Realizing the significance of the higher-order contribution, we extended our dynamic dipole polarizability to the higher-order dynamic multipole polarizability.[61] Judging with the MARE for each order coefficient for atom pairs, this extension is

nearly perfect, although it is not trivial. For convenience, we call these two models the solid-sphere model. While the solid-sphere model can achieve excellent accuracy for usual quasispherical systems, it fails to describe cage molecules that have a concentric cavity such as fullerenes. To address this issue, we developed a classical shell model.[62] This model allows us to calculate the vdW coefficients for all orders. It was shown[64] that, within the classical shell model, the all-order perturbative contribution can be summed up analytically. The model has been applied to study the asymptotic dependence of vdW coefficients upon cluster size.

2. Dynamic Dipole Polarizability and Leading-Order vdW Coefficient

In this section, we discuss several models for the dynamic dipole polarizability. Then we compare their performance on the vdW coefficient C_6 for rare-gas dimers, the standard model systems for the vdW interaction.

2.1. *Solid-sphere model*

The starting point of the solid-sphere dynamic dipole model[58] is a classical conducting solid sphere of radius R, with the electron density uniform inside and zero outside the sphere. The exact expression for the dynamic dipole polarizability of this paradigm density is given by[65,66]:

$$\alpha_1(iu) = \left[\frac{\epsilon - 1}{\epsilon + 2}\right] R^3 \,, \tag{7}$$

where ϵ is the dielectric function of the conducting sphere of uniform density. In the short wave vector (or long wavelength) limit, $\epsilon = 1 + \omega_p^2/u^2$. Substituting the dielectric function into Eq. (7) leads to:

$$\alpha_1(iu) = \left(\frac{\omega_1^2}{\omega_1^2 + u^2}\right) R^3 \,. \tag{8}$$

Here ω_1 is the dipole resonance frequency of the sphere given by $\omega_1 = \omega_p\sqrt{1/3}$, with $\omega_p = \sqrt{4\pi n}$ being the plasmon frequency of the extended uniform electron gas and n being the electronic density of the sphere under consideration. (hartree atomic units $e^2 = \hbar = m = 1$ are used from now on unless otherwise explicitly stated.)

In order to make our model accurate for both molecules and solids, we should respect the paradigm densities in both condensed matter physics (slowly varying densities) and quantum chemistry (compact one- or two-electron densities). We should also respect the high-frequency ($u \to \infty$) limit, which is given by[67]:

$$\alpha_1(\omega) \to \int d\mathbf{r} n(\mathbf{r})/u^2 \,. \tag{9}$$

and the zero-frequency or static limit, $\alpha_1(0)$, of the dynamic dipole polarizability. All these conditions may be satisfied by assuming that the dynamic dipole polariz-

ability for an inhomogeneous density takes the form of:

$$\alpha_1(iu) = \frac{3}{4\pi d_1}\int d^3r\Theta(R_1 - r)\frac{d_1^4\omega_1^2}{d_1^4\omega_1^2 + u^2}\,, \tag{10}$$

where $\Theta(x)$ is a step function: $\Theta(x) = 1$ for $x > 0$ and $\Theta(x) = 0$ for $x \leq 0$. To ensure the satisfaction of the high-frequency as well as the static limit conditions, two parameters were introduced. They are determined as follows. In the static limit, we require that the correct dipole polarizability be reproduced. This yields

$$\alpha_1(0) = \frac{3}{4\pi d_1}\int d\mathbf{r}\Theta(R_1 - r)\,. \tag{11}$$

For spherically-symmetric densities, we immediately obtain

$$R_1 = [d_1\alpha_1(0)]^{1/3}. \tag{12}$$

In the high-frequency limit, we require that the exact dipole polarizability be reproduced, leading to:

$$d_1 = \left[\frac{\int_0^\infty dr4\pi r^2 n(r)}{\int_0^{R_1} dr4\pi r^2 n(r)}\right]^{1/3} \geq 1\,. \tag{13}$$

For the classical conducting sphere of uniform density, the radius of the sphere is fixed to be R. For such a density, $R_1 = R$. So we have $d_1 = 1$.

For the dipole–dipole interaction, we set $l_1 = l_2 = 1$ in Eq. (3). Then we have

$$C_6^{\mathrm{AB}} = \frac{3}{\pi}\int_0^\infty du\alpha_1^{\mathrm{A}}(iu)\alpha_1^{\mathrm{B}}(iu)\,. \tag{14}$$

Substituting Eq. (10) into Eq. (14) and performing the integration over u (the magnitude of imaginary frequency iu) yield the leading-order vdW coefficient

$$C_6 = \frac{27d_{1\mathrm{A}}d_{1\mathrm{B}}}{32\pi^2}\int d^3r_{\mathrm{A}}\Theta_1^{\mathrm{A}}\int d^3r_{\mathrm{B}}\Theta_1^{\mathrm{B}}\frac{\omega_1(r_{\mathrm{A}})\omega_1(r_{\mathrm{B}})}{d_{1\mathrm{A}}^2\omega_1(r_{\mathrm{A}}) + d_{1\mathrm{B}}^2\omega_1(r_{\mathrm{B}})}\,, \tag{15}$$

where $\Theta = \Theta(R_1 - r)$ and R_1 is the cutoff radius which can be calculated from the static dipole polarizability [see Eq. (12)].

To see whether the dynamic dipole polarizability of Eq. (10) is accurate enough for the one- or two-electron densities, the paradigm in quantum chemistry, the dynamic dipole polarizabilities of the H and He atoms were calculated with Eq. (10) using the ground-state density of these two atoms. Figure 1 shows the comparison of the dynamic dipole polarizability of the H atom obtained from the solid-sphere model to the exact one.[68] To further compare its accuracy with other approximations, we also plot the Andersson–Langreth–Lundqvist dynamic dipole polarizability of the H atom in Fig. 1. From Fig. 1, we observe that the solid-sphere model agrees very well with the exact one over the whole range of frequency and is much more accurate than the Andersson–Langreth–Lundqvist model.[50] The equally excellent agreement between the solid-sphere model and the highly-accurate wave

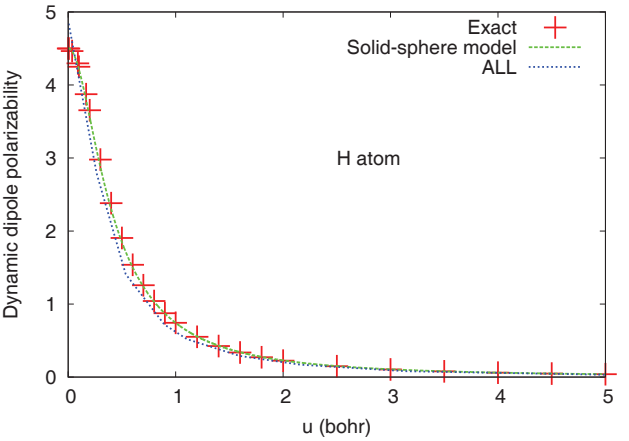

Fig. 1. (Color online) Dynamic dipole polarizability $\alpha_j(iu)$ (in atomic units) of the H atom: Exact, solid-sphere model (Eq. (10) with $d_1 = 1.143$ and $R_1 = 1.726$) and ALL.[50]

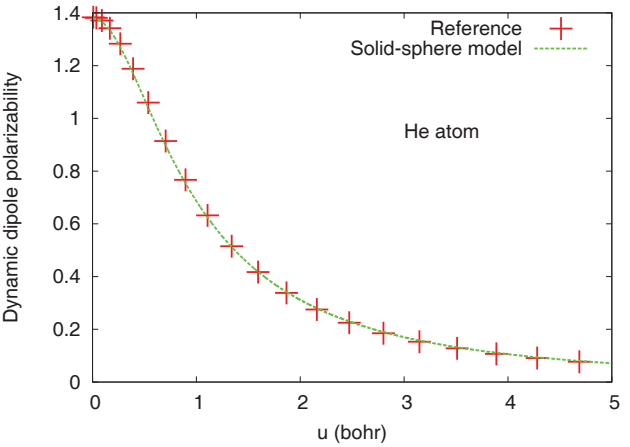

Fig. 2. (Color online) Dynamic dipole polarizability $\alpha_1(iu)$ (in atomic units where $e^2 = \hbar = m = 1$) of the He atom: reference value[68] (red) and present model (green). $\omega = iu$ is the imaginary frequency.

function-based dynamic dipole polarizability[68] for the He atom is also observed in Fig. 2. This suggests that the solid-sphere model is not only correct for the paradigm density in condensed matter physics, but also accurate for paradigm densities in quantum chemistry.

As a simple test, we calculated[58] C_6 for diverse atom pairs with Eq. (15). In our calculations, spin-restricted Hartree–Fock densities[69] are used. (The dynamic dipole polarizability is not sensitive to the electron density. So, it should not make much difference if DFT densities, which include the electron correlation, are used.) The inputs for the true static dipole polarizabilities $\alpha(0)$ are listed in Table 1.

Table 1. Static multipolar polarizabilities $\alpha_l(0)$ and cutoff radii R_l (both in atomic units) and parameters a_l of atoms. For the H atom, the Bohr radius is 1.00, a conventional vdW radius is $\alpha_1(0)^{1/3} = 1.65$ and the classical turning radius is 2.00.

Atom	$\alpha_1(0)$	$\alpha_2(0)$	$\alpha_3(0)$	R_1	R_2	R_3	d_1	d_2	d_3
H	4.50[a]	15.0[a]	131.25[a]	1.726	1.856	2.194	1.143	1.469	1.863
He	1.38[b]	2.331[d]	9.932[d]	1.155	1.268	1.508	1.116	1.405	1.784
Ne	2.67[b]	7.33[e]	42.1[e]	1.409	1.545	1.794	1.047	1.200	1.422
Ar	11.1[b]	51.84[f]	534.85[f]	2.249	2.277	2.564	1.025	1.180	1.364
Kr	16.8[b]	98.43[f]	1269.6[f]	2.571	2.574	2.892	1.012	1.149	1.332
Xe	27.4[b]	223.3[e]	3640.6[e]	3.023	3.020	3.348	1.008	1.124	1.296
Li	164.1[c]	1424[g]	39688[g]	5.507	4.526	4.888	1.018	1.333	1.680
Na	162.6[c]	1878[g]	55518[g]	5.470	4.719	5.128	1.006	1.246	1.679
K	290.2[c]	5000[g]	176940[g]	6.629	5.682	6.033	1.004	1.184	1.645
Be	37.8[b]	299.9[d]	4765[d]	3.401	3.298	3.590	1.041	1.301	1.613
Mg	71.7[b]	845.4[d]	16772[d]	4.171	4.007	4.276	1.012	1.222	1.559
Ca	158.6[b]	3083[e]	65170[e]	5.425	5.143	5.190	1.007	1.168	1.557

[a]Ref. 70, [b]Ref. 71, [c]Ref. 72, [d]Ref. 73, [e]Ref. 74, [f]Ref. 75, [g]Ref. 76.

The results are tabulated in Table 2. From Table 2 we can see that this model is remarkably accurate with a MARE of only 3%.

This model can be applied to study the vdW coefficient C_6^+ between ion cores in alkali metals. The screening effect of valence electrons on ion core interaction can be accounted for with a simple formula derived by Rehr *et al.*,[84] who showed that, to a good approximation, one could use the long-wavelength limit of the dynamic dielectric function of the uniform valence-electron density (with plasma frequency $\Omega_p = (4\pi n_{\text{valence}})^{1/2}$). For any core–core pair interaction, we have[58]:

$$C_6^+ = \frac{27 d_1 d_2}{32\pi^2} \int d\mathbf{r}_1 \Theta_1 \int d\mathbf{r}_2 \Theta_2 \frac{\tilde{\omega}_{\text{p}}(\mathbf{r}_1)\tilde{\omega}_{\text{p}}(\mathbf{r}_2) S(\mathbf{r}_1, \mathbf{r}_2)}{d_1^2 \tilde{\omega}_{\text{p}}(\mathbf{r}_1) + d_2^2 \tilde{\omega}_{\text{p}}(\mathbf{r}_2)}, \tag{16}$$

$$S = \frac{\Omega_{\text{p}} \tilde{\omega}_{\text{p}}(\mathbf{r}_1)\tilde{\omega}_{\text{p}}(\mathbf{r}_2)[d_1^2 \tilde{\omega}_{\text{p}}(\mathbf{r}_1) + d_2^2 \tilde{\omega}_{\text{p}}(\mathbf{r}_2)]/2 + [d_1 d_2 \tilde{\omega}_{\text{p}}(\mathbf{r}_1)\tilde{\omega}_{\text{p}}(\mathbf{r}_2)]^2}{(d_1 d_2)^{-2}[\Omega_{\text{p}} + a_1^2 \tilde{\omega}_{\text{p}}(\mathbf{r}_1)]^2 [\Omega_{\text{p}} + a_2^2 \tilde{\omega}_{\text{p}}(\mathbf{r}_2)]^2},$$

where d_1 is given by Eq. (13) and S accounts for the screening of valence electrons on the core–core interaction. For like-pair ionic interactions,[58] $d_1 = d_2 = d$. Eq. (16) reduces to

$$C_6^+ = \frac{27}{32\pi^2} \int d\mathbf{r}_1 \Theta_1 \int d\mathbf{r}_2 \Theta_2 \frac{\tilde{\omega}_{\text{p}}(\mathbf{r}_1)\tilde{\omega}_{\text{p}}(\mathbf{r}_2)}{\tilde{\omega}_{\text{p}}(\mathbf{r}_1) + \tilde{\omega}_{\text{p}}(\mathbf{r}_2)} S(\mathbf{r}_1, \mathbf{r}_2),$$

$$S = \frac{d^6 \tilde{\omega}_{\text{p}}(\mathbf{r}_1)\tilde{\omega}_{\text{p}}(\mathbf{r}_2)\{\Omega_p[\tilde{\omega}_{\text{p}}(\mathbf{r}_1) + \tilde{\omega}_{\text{p}}(\mathbf{r}_2)]/2 + d^2 \tilde{\omega}_{\text{p}}(\mathbf{r}_1)\tilde{\omega}_{\text{p}}(\mathbf{r}_2)\}}{[\Omega_p + d^2 \tilde{\omega}_{\text{p}}(\mathbf{r}_1)]^2 [\Omega_p + d^2 \tilde{\omega}_{\text{p}}(\mathbf{r}_2)]^2}.$$

The accuracy of our C_6^+ was tested for free like-ion pairs, for which $S = 1$, using the static polarizabilities[85,86] of the free ions. It was found that C_6^+ calculated with the solid-sphere model are lower than those estimated[86] with the adiabatic

Table 2. The vdW coefficients C_6 (in atomic units) calculated with Eq. (15) using spin-restricted Hartree–Fock densities.[69] The mean absolute relative error is 3.2%.

	Reference	Present		Reference	Present
He–He	1.46[a]	1.44	Ar–H	19.9[b]	19.8
Ne–Ne	6.55[b]	7.33	Ar–Li	174[h]	180
Ar–Ar	65.8[a]	67.7	Ar–Na	197[h]	200
Kr–Kr	133[a]	133	Ar–K	299[h]	315
Xe–Xe	302[b]	296	Kr–H	29.1[b]	28.1
He–Ne	3.07[b]	3.20	Kr–Li	260[h]	267
He–Ar	9.57[b]	9.78	Kr–Na	293[h]	294
He–Kr	13.7[b]	13.6	Kr–K	444[h]	463
He–Xe	19.9[b]	20.0	Xe–H	44.1[b]	42.5
Ne–Ar	19.8[b]	21.4	Xe–Li	411[h]	423
Ne–Kr	28.0[b]	29.6	Xe–Na	461[h]	462
Ne–Xe	40.5[b]	43.3	Xe–K	698[h]	727
Ar–Kr	93.2[b]	94.7	He–Be	13.0[g]	13.6
Ar–Xe	138[b]	141	He–Mg	21.1[g]	21.3
Kr–Xe	201[b]	198	He–Ca	36.6[i]	37.2
H–H	6.50[c]	6.28	Ne–Be	27.5[a]	27.8
Li–Li	1388[d]	1335	Ne–Mg	42.9[a]	43.6
Na–Na	1472[d]	1404	Ne–Ca	72.0[i]	75.7
K–K	3813[d]	3655	Ar–Be	102[a]	102
H–Li	66.5[e]	67.2	Ar–Mg	162[a]	159
H–Na	74.2[e]	72.5	Ar–Ca	274[i]	280
H–K	112[e]	114	Kr–Be	149[a]	147
Li–Na	1427[d]	1366	Kr–Mg	238[a]	232
Li–K	2293[d]	2184	Kr–Ca	404[i]	408
Na–K	2348[d]	2258	Xe–Be	228[a]	227
Be–Be	213[f]	215	Xe–Mg	367[a]	359
Mg–Mg	630[f]	583	Xe–Ca	630[i]	636
Ca–Ca	2188[f]	2057	H–Be	34.4[b]	34.9
Be–Mg	365[f]	352	H–Mg	57.8[b]	55.4
Be–Ca	661[f]	646	H–Ca	100[i]	98.6
Mg–Ca	1158[f]	1086	Li–Be	478[f]	476
He–H	2.81[g]	2.75	Li–Mg	857[f]	823
He–Li	22.5[e]	23.3	Li–Ca	1688[f]	1608
He–Na	25.8[e]	26.2	Na–Be	521.6[f]	500
He–K	39.5[e]	41.4	Na–Mg	930[f]	859
Ne–H	5.69[b]	5.78	Na–Ca	1814[f]	1668
Ne–Li	43.8[h]	46.30	K–Be	791[f]	787
Ne–Na	50.4[h]	52.8	K–Mg	1417[f]	1358
Ne–K	77.4[h]	83.7	K–Ca	2803[f]	2655

[a]Ref. 75, [b]Ref. 74, [c]Ref. 77, [d]Ref. 76, [e]Ref. 78, [f]Ref. 79, 80, [g]Ref. 81, [h]Ref. 82, [i]Ref. 83.

local density approximation (ALDA), as shown in Table 3. Since the static dipole polarizability of the free ion cores evaluated with TDDFT-ALDA is systematically higher than the experimental values,[86] probably the TDDFT-ALDA values of C_6^+ are also overestimated.

Table 3. C_6 for free core–core interaction of alkali atoms. Atomic units are used. The adiabatic TDDFT-LDA values are taken from Ref. 86.

Solid	Eq. (15)	TDDFT-ALDA
Li^+	0.072	
Na^+	1.69	1.67
K^+	19.5	23.3
Rb^+	43.5	54.0
Cs^+	104	

In summary, we used constraint satisfaction to construct a well-motivated nonlocal density functional for the long-range vdW interaction, which correctly reduces to the uniform-gas limit for slowly-varying densities.

2.2. *Comparative study of the vdW coefficients*

To further assess the performance of the solid-sphere dipole model, a comparison is made between the solid-sphere model and several density functional-type methods, including the nonempirical Andersson–Langreth–Lundqvist[50] and Becke–Johnson[55,56] methods as well as the empirical or semiempirical VV10[59] and Lima–Caldas[53] models. A brief discussion of these methods is given below.

The Andersson–Langreth–Lundqvist method is based on the work of Rapcewicz and Ashcroft,[49] whose starting point is the interaction between two pieces of uniform density that belong to the extended uniform electron gas. Since the two interacting objects may have different electron densities, Rapcewicz and Ashcroft chose $\sqrt{n(\mathbf{r}_1)n(\mathbf{r}_2)}$ as the effective uniform density for the system consisting of two subsystems A and B, i.e., $n_{\text{eff}} = \sqrt{n(\mathbf{r}_1)n(\mathbf{r}_2)}$, with $n(\mathbf{r}_1)$ and $n(\mathbf{r}_2)$ representing uniform densities of two interacting subsystems, respectively. However, Andersson, Langreth and Lundqvist found that a better choice of the effective density should be:

$$n_{\text{eff}} = \left[\sqrt{n(\mathbf{r}_1)n(\mathbf{r}_2)}\left(\sqrt{n(\mathbf{r}_1)} + \sqrt{n(\mathbf{r}_2)}\right)/2\right]^{2/3}. \tag{17}$$

This leads to the dynamic dipole polarizability:

$$\alpha_1(iu) = \frac{1}{4\pi}\int d^3r\ \frac{\omega_p^2}{\omega_p^2 + u^2} \tag{18}$$

and the vdW coefficient

$$C_6 = \frac{3}{32\pi^2}\int d^3r_{\text{A}}\int d^3r_{\text{B}}\frac{\omega_p(\mathbf{r}_{\text{A}})\omega_p(\mathbf{r}_{\text{B}})}{\omega_p(\mathbf{r}_{\text{A}}) + \omega_p(\mathbf{r}_{\text{B}})}. \tag{19}$$

Numerical tests show that the Andersson–Langreth–Lundqvist model of Eq. (19) is more accurate than that of Rapcewicz and Ashcroft. This model requires a sharp cutoff of plasmon contribution which is implicitly implemented with the spatial

integral of Eq. (19). This cutoff procedure is the same as that used in Rapcewicz-Ashcroft model. The input of the model is the true electron density, which may be accessible in every DFT calculation.

Becke and Johnson[55,56] proposed a series of methods for the calculation of vdW coefficients, on the basis of the exchange hole. The latest version provides a nonempirical derivation of the method. The starting point of this method is the exchange hole dipole moment, which is defined by

$$d_{X\sigma}(\mathbf{r}_1) = \left[\frac{1}{n_\sigma(\mathbf{r}_1)}\Sigma_{ij}\psi_{i\sigma}(\mathbf{r}_1)\psi_{j\sigma}(\mathbf{r}_1)\int d^3r_2\mathbf{r}_2\psi_{i\sigma}(\mathbf{r}_2)\psi_{j\sigma}(\mathbf{r}_2)\right] - \mathbf{r}_1\,, \qquad (20)$$

where $\mathbf{r}_1$ is the position of an electron of spin σ and $\mathbf{r}_2$ is the position where the associated exchange hole is located. It deletes the probability of finding another electron of spin σ at $\mathbf{r}_2$, given an electron of spin σ at $\mathbf{r}_1$, due to the Pauli exclusion principle. $\psi_{i\sigma}$ are the Kohn–Sham orbitals occupied with an electron of spin σ.

From the exchange hole dipole moment, the multipole moment due to the negatively-charged electron e^- and the corresponding positively-charged exchange hole e^+ can be calculated from

$$M_{l\sigma} = -\{r^l - [r - d_{X\sigma}(r)]^l\}\,, \qquad (21)$$

with $l = 1$ representing the dipole. Here r is the distance of the electron from the nucleus of an atom. According to second-order perturbation theory, Becke and Johnson finally expressed the vdW coefficient in terms of the expectation value of the multipole moment of Eq. (21) and the average excitation energy. Then they evaluated the average excitation energy from the static dipole polarizability. The required input of this approach is the static dipole polarizability and the single-particle orbitals, which are accessible from Hartree–Fock or DFT calculations.

Vydrov and van Voorhis[59] proposed a dynamic dipole polarizability. The starting point of this model is the Clausius–Mossotti formula:

$$\alpha_1 = \frac{3}{4\pi}\frac{\epsilon - 1}{\epsilon + 2}\,, \qquad (22)$$

where α_1 is the dipole polarizability of a solid sphere of uniform density and ϵ is the dielectric function. Then the formula is generalized to an inhomogeneous electron gas. For a semiconductor with a band gap ω_g, to a good approximation, the dielectric function in the long wavelength (i.e., zero wave vector) limit is assumed to be[87]:

$$\epsilon(iu) = 1 + \frac{\omega_p^2}{\omega_g^2 + u^2}\,. \qquad (23)$$

This expression is exact for a nearly-free electron gas. Substituting Eq. (23) into Eq. (22) leads to:

$$\alpha_1(\mathbf{r}, iu) = \left(\frac{3}{4\pi}\right)\frac{\omega_p^2(\mathbf{r})/3}{\omega_p^2(\mathbf{r})/3 + \omega_g^2(\mathbf{r}) + u^2}\,. \qquad (24)$$

Here the position-dependent $\alpha_1(\mathbf{r}, iu)$ is called the local dynamic dipole polarizability. Then the (global) dynamic dipole polarizability can be obtained from

$$\alpha_1(iu) = \int d^3r \; \alpha_1(\mathbf{r}, iu) \,. \tag{25}$$

This formula recovers the exact expression of Eq. (7) for the dynamic dipole polarizability of a classical conducting solid sphere of uniform density, for which the local band gap $\omega_g(\mathbf{r})$ vanishes. Now the spatial integration is finite unless $\omega_g(\mathbf{r})$ is zero. Therefore, the VV10 model does not require any imposed cutoff condition, because the local band gap $\omega_g(\mathbf{r})$ can provide a smooth cutoff. The local band gap can be constructed as follows.

In the density tail, the density has an exponential decay,

$$n(\mathbf{r}) \sim \exp(-\alpha|\mathbf{r}|) \,, \tag{26}$$

where $\alpha = 2\sqrt{2I}$, with I being the ionization potential. For a two-electron exponential density, the ionization potential can be expressed as:

$$I = \frac{1}{8}\left|\frac{\nabla n(\mathbf{r})}{n(\mathbf{r})}\right|^2 . \tag{27}$$

Generalization of Eq. (27) to a system of many electrons leads to the assumption:

$$I(\mathbf{r}) = \frac{1}{8}\left|\frac{\nabla n(\mathbf{r})}{n(\mathbf{r})}\right|^2 . \tag{28}$$

VV called $I(\mathbf{r})$ the local ionization potential. Assuming that the local band gap is proportional to the local ionization potential, i.e., $\omega_g(\mathbf{r}) \propto I(\mathbf{r})$, VV suggested that:

$$\omega_g^2(\mathbf{r}) = C\left|\frac{\nabla n(\mathbf{r})}{n(\mathbf{r})}\right|^4 , \tag{29}$$

where $C = 0.0089 = (0.0943)^2$ is the proportionality coefficient, which was fixed by a fit to the reference values of a small set of vdW coefficients. This coefficient is very close to the value 9/1024 that reproduces the exact ionization potential of the H atom.

VV10 dynamic dipole polarizability is a smooth function of $\mathbf{r}$, due to the smooth cutoff. It does not recover the correct static limit, although it is exact in the high-frequency limit. This violation has been partly fixed by introducing the empirical parameter C.

Lima and Caldas[53] proposed a dynamic dipole polarizability for an atom. The accuracy of this model relies on empirical adjustment of several parameters. It respects both the static and high-frequency limits. The starting point of the Lima–Caldas model is the assumption

$$\alpha_1(iu) = \int d^3r \; \chi(n(r), iu) \,, \tag{30}$$

where $\chi(n, iu)$ is the angle average of the electric susceptibility and $n(r)$ is the spherical average of the electron density. Clearly this assumption is equivalent to

that of VV10 [see Eq. (25)]. In order to satisfy the high-frequency limit, Lima and Caldas proposed:

$$\chi(n(r), iu) = \frac{\chi(n(r), 0)}{[1 + [\chi(n(r), 0)/n(r)]u^2]}, \tag{31}$$

where $\chi(n(r), 0)$ is the static electric susceptibility. For the uniform electron gas, it is given by:

$$\chi(n, 0) = \frac{3}{4\pi}. \tag{32}$$

However, for an inhomogeneous electron gas, this quantity is in general unknown and an approximation has to be made. Lima and Caldas proposed a density functional-like approximation:

$$\chi(n(r), 0) = \frac{\alpha_1(0)n(r)/[n_\alpha + n(r)]}{\int d^3r\ n(r)/[n_\alpha + n(r)]}. \tag{33}$$

Table 4. Comparison of different models for the vdW coefficients C_6 (in atomic units). SSM = solid-sphere model, BJ = Becke–Johnson, LC = Lima–Caldas and ALL = Andersson–Langreth–Lundqvist. MARE = mean absolute relative error.

Atom pair	Reference[a]	SSM[a]	BJ[b]	ALL[c]	LC[d]	VV09[e]	vdW-DF[f]	vdW-DF2[g]
He–He	1.46	1.44	1.64	2.0	1.46	1.45	2.93	0.76
Ne–Ne	6.55	7.35	5.83	6.0	6.33	8.44	9.45	3.07
Ar–Ar	65.8	67.8	62.7	63.0	66.3	70.1	62.7	25.3
Kr–Kr	133	132	132	123	127	131	114	47.7
Xe–Xe	302	295	305	260	278			
He–Ne	3.07	3.22	3.09	3.5	3.03			
He–Ar	9.57	9.81	9.81	11.0	9.72			
He–Kr	13.7	13.6	14.1	15.5	13.3			
He–Xe	19.9	20.0	20.9	22.0	19.2			
Ne–Ar	19.8	21.5	18.6	18.5	20.0			
Ne–Kr	28.0	29.6	26.7	25.0	27.1			
Ne–Xe	40.5	43.3	39.7	35.5	39.2			
Ar–Kr	93.2	94.4	90.9	87.5	91.5			
Ar–Xe	138	140	137	127	134			
Kr–Xe	201	197	200	178	187			
H–H	6.50	6.28	6.76	6.0	6.50	6.75		
H–He	2.81	2.75	2.99	3.0				
H–Ne	5.69	5.79	5.69	5.0				
H–Ar	19.9	19.8	20.1	18.5				
H–Kr	29.1	28.0	29.4	26.0				
H–Xe	44.1	42.4	45.1	38.0				
MARE		3%	3%	12%				

[a]From Table 2. [b]From Ref. 55. [c]From Ref. 50. [d]From Ref. 53. [e]From Ref. 59. In the large-separation limit, it was found[59] that VV09 [O. A. Vydrov and T. Van Voorhis, *Phys. Rev. Lett.* **103**, 063004 (2009).] reduces to VV10. [f]From Ref. 59. For vdW-DF, see M. Dion, H. Rydberg, E. Schroeder, D. C. Langreth and B. I. Lundqvist, *Phys. Rev. Lett.* **92**, 246401 (2004). [g]From Ref. 59. For vdW-DF2, see K. Lee, E. D. Murray, L. Kong, B. I. Lundqvist and D. C. Langreth, *Phys. Rev. B* **82**, 081101 (2010).

Here $\alpha_1(0)$ is the static dipole polarizability and n_α is the electron density at the vdW radius of an atom, which is conventionally defined by $R = [\alpha_1(0)]^{1/3}$. To improve the accuracy of C_6 for atom pairs, Lima and Caldas further introduced a density-dependent function $f^S(n)$ into $\chi(n,0)$. The final form of $\chi(n,0)$ is written as:

$$\chi(n,0) = \frac{\alpha_1(0)n(r)f^S(n)/[n_\alpha + n(r)]}{\int d^3r\ n(r)f^S(n)/[n_\alpha + n(r)]}\,. \tag{34}$$

While good improvement can be achieved with this approximation, the physics behind the construction of $f^S(n)$ is not so clear. As a result, when the formula for the dynamic dipole polarizability is generalized to higher-order dynamic multipole polarizability,[54] more empirical parameters have to be introduced to retain the accuracy of the dynamic dipole polarizability.

Table 4 shows the comparison of several models to the accurate reference values. From Table 4 we see that both Becke–Johnson and our solid-sphere models can achieve the accuracy of the empirical model of Lima and Caldas.

3. Dynamic Multipole Polarizability and Higher-Order Coefficients

The original motivation for developing a model for higher-order dynamic multipole polarizability is the calculation of higher-order vdW coefficients such as C_8 and C_{10}. The model is a simple extension of the solid-sphere dynamic dipole polarizability.[58] The only needed input are the static multipole polarizabilities and the electron density. The extension does not need empirical fitting. The nonlocal density functional for the dynamic multipole polarizability was modeled in a way that it is exact in the zero- and high-frequency limits, exact in the uniform-gas limit and accurate for the one- and two-electron densities. So, the model may be regarded as an interpolation between those limits in a way that is exact for a paradigm density from textbooks on classical electromagnetism: the metal sphere of uniform density. Because the frequency-dependence of the model dynamic multipole polarizability is simple, our formula transfers with little error from the paradigm density to the density of a real spherical system such as an atom.

Let us consider a classical conducting solid sphere of uniform density of radius R (which is small enough so that retardation effect can be neglected), in empty space. The dynamic multipole polarizability of the metallic solid sphere is given by[88]:

$$\alpha_l(iu) = \left[\frac{\epsilon - 1}{\epsilon + (l+1)/l}\right] R^{2l+1}\,, \tag{35}$$

where ϵ is the dielectric function of the sphere. By setting $\epsilon = 1 + \omega_p^2/u^2$ (the long wavelength limit of an isotropic media), we find

$$\alpha_l(iu) = \left(\frac{\omega_l^2}{\omega_l^2 + u^2}\right) R^{2l+1}\,. \tag{36}$$

Here ω_l is the multipole resonance frequency of the sphere given by $\omega_l = \omega_p\sqrt{l/(2l+1)}$. A familiar limit of Eq. (36) is the static dipole polarizability R^3.

Now we make a nonempirical model for $\alpha_l(iu)$ in terms of the electron density, by imposing exact constraints on a simple expression. First, we demand recovery of the correct zero-frequency limit $\alpha_l(0)$. Second, we demand recovery of the correct high-frequency ($u \to \infty$) limit,[54,79,80]

$$\alpha_l(iu) \to l \int_0^\infty dr\ 4\pi r^2 n(r) r^{2l-2} \Big/ u^2 \,. \tag{37}$$

Third, we make our expression exact[88–90] for a classical conducting solid sphere of uniform density inside and zero density outside a radius R [see Eq. (36)]. Taking all three conditions into consideration, our model dynamic multipole polarizability of any spherical density was assumed to be

$$\alpha_l(iu) = \frac{1}{4\pi d_l}\left(\frac{2l+1}{l}\right)\int d^3r \Theta(R_l - r)\frac{l r^{2l-2}\ d_l^4\omega_l^2}{d_l^4\omega_l^2 + u^2} \,. \tag{38}$$

The classical conducting solid sphere has a natural sharp cutoff of all integrals over r, which we extend even to the diffuse density of an atom. Unbiased sharp cutoffs are also used in the construction of nonempirical density functionals for the exchange-correlation energy[91–93] and a model dynamic dipole polarizability.[50] The parameter d_l and the cutoff radius R_l are determined by the two imposed constraints. According to the static limit condition, we have

$$\alpha_l(0) = \frac{2l+1}{4\pi d_l}\int d^3r\ r^{2l-2}\ \Theta(R_l - r) \,. \tag{39}$$

Without the cutoff, the right-hand side of Eq. (39) would diverge. For spherically-symmetric systems, the radial cutoff is

$$R_l = [d_l \alpha_l(0)]^{1/(2l+1)} \,. \tag{40}$$

Imposing the high-frequency limit of Eq. (37) leads to

$$d_l = \left[\frac{\displaystyle\int_0^\infty dr\ 4\pi r^2\ r^{2l-2}\ n(r)}{\displaystyle\int_0^{R_l} dr\ 4\pi r^2\ r^{2l-2}\ n(r)}\right]^{1/3} \geq 1 \,. \tag{41}$$

For a metallic sphere of uniform density with radius R, we find $d_l = 1$ and $R_l = R$. Then Eq. (38) correctly reduces to Eq. (36). Since Eqs. (40) and (41) are coupled together, in general they must be solved self-consistently. The two parameters obtained for atoms are displayed in Table 1. From Table 1 we see that there is a relationship among the parameters d_l: $d_1 < d_2 < d_3$. This is because, if we keep the same cutoff radius for different order l, the denominator will get smaller relative to the numerator as l increases, due to the cutoff. One desired feature of the present model is that, for $l = 1$, our expressions reduce to those of the model dynamic dipole polarizability discussed above.[58]

The central idea in developing the dynamic multipole polarizability is parallel to the one that has been used before to construct nonemprical density functionals for the exchange-correlation energy[16,17,94] : Make the functional exact for paradigm densities and satisfy other exact constraints for a broader class of densities of interest. We believe that our use of a paradigm density (the classical conducting solid sphere or "local density approximation" in the vdW DFT) is what leads to accurate higher-order vdW coefficients without empiricism.

4. Application to Atom–Atom Pair Interaction

We apply the present model to calculate the dynamic multipole polarizabilities of the H atom and compare them to the corresponding exact values.[70] Similar to the case for the dynamic dipole polarizability, we observe from Figs. 3 and 4 that our model dynamic multipole polarizabilities are in excellent agreement with the exact values within the whole range of frequencies. We also apply it to the He atom. As shown in Figs. 5 and 6, the deviation of the solid-sphere model from the accurate reference values obtained from the highly-accurate many-body calculations[68,77] is nearly indistinguishable.

4.1. *vdW coefficients*

The higher-order vdW coefficients C_8 and C_{10} may be obtained by substituting the model dynamic multipole polarizabilities [Eqs. (38), (40) and (41)] into the exact expression given by Eq. (3). Performing the frequency integration of Eq. (3)

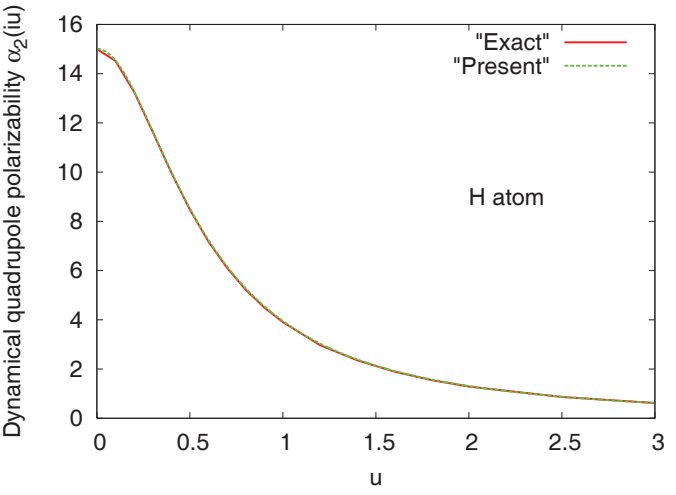

Fig. 3. (Color online) Dynamical quadrupole polarizability $\alpha_1(iu)$ (in atomic units) of the H atom: reference value[68] (red) and present model (green). $\omega = iu$ is the imaginary frequency.

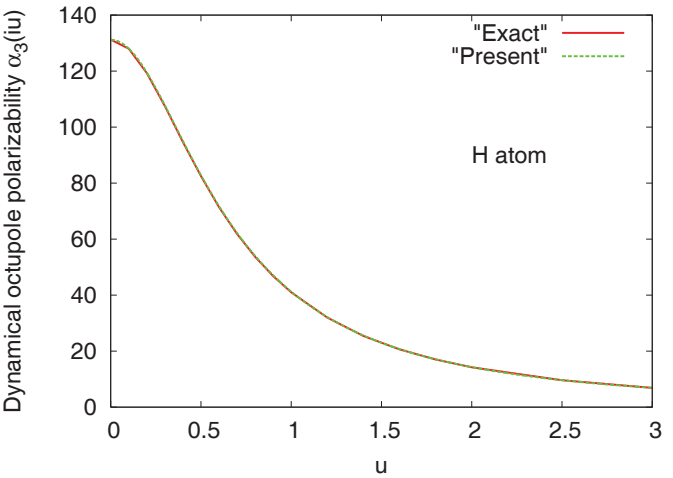

Fig. 4. (Color online) The same as Fig. 3, but for octupole polarizability.

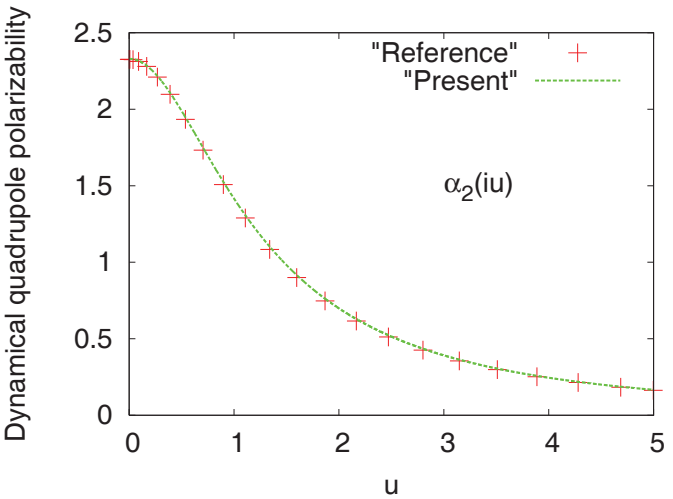

Fig. 5. (Color online) Dynamical quadrupole polarizability $\alpha_1(iu)$ (in atomic units where $e^2 = \hbar = m = 1$) of the He atom: reference value[68] (red) and present model (green). $\omega = iu$ is the imaginary frequency.

analytically yields the final expressions for C_8 and C_{10}. The results are:

$$C_8 = \frac{225 d_{1\mathrm{A}} d_{2\mathrm{B}}}{64\pi^2} \int d^3 r_{\mathrm{A}}\ \Theta_1^{\mathrm{A}} \int d^3 r_{\mathrm{B}}\ \Theta_2^{\mathrm{B}} \frac{r_{\mathrm{B}}^2 \omega_1(r_{\mathrm{A}}) \omega_2(r_{\mathrm{B}})}{d_{1\mathrm{A}}^2 \omega_1(r_{\mathrm{A}}) + d_{2\mathrm{B}}^2 \omega_2(r_{\mathrm{B}})}$$
$$+ \frac{225 d_{2\mathrm{A}} d_{1\mathrm{B}}}{64\pi^2} \int d^3 r_{\mathrm{A}}\ \Theta_2^{\mathrm{A}} \int d^3 r_{\mathrm{B}}\ \Theta_1^{\mathrm{B}} \frac{r_{\mathrm{A}}^2 \omega_2(r_{\mathrm{A}}) \omega_1(r_{\mathrm{B}})}{d_{2\mathrm{A}}^2 \omega_2(r_{\mathrm{A}}) + d_{1\mathrm{B}}^2 \omega_1(r_{\mathrm{B}})}\,, \qquad (42)$$

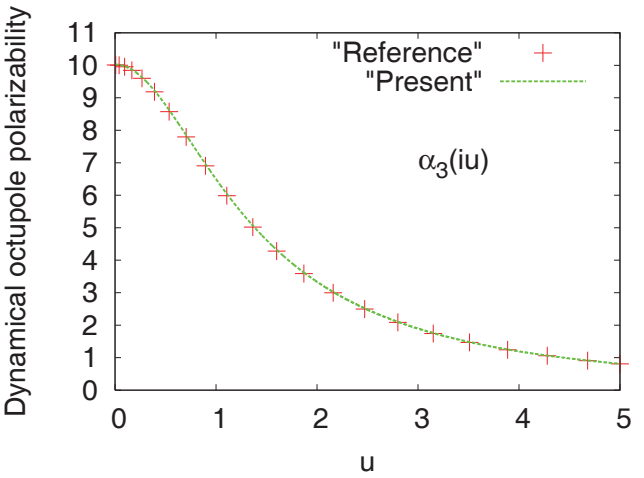

Fig. 6. (Color online) The same as Fig. 5, but for octupole polarizability.

$$C_{10} = \frac{441 d_{1\mathrm{A}} d_{3\mathrm{B}}}{48\pi^2} \int d^3 r_{\mathrm{A}}\ \Theta_1^{\mathrm{A}} \int d^3 r_{\mathrm{B}}\ \Theta_3^{\mathrm{B}} \frac{r_{\mathrm{B}}^4 \omega_1(r_{\mathrm{A}})\omega_3(r_{\mathrm{B}})}{d_{1\mathrm{A}}^2 \omega_1(r_{\mathrm{A}}) + d_{3\mathrm{B}}^2 \omega_3(r_{\mathrm{B}})}$$
$$+ \frac{441 a_{3\mathrm{A}} d_{1\mathrm{B}}}{48\pi^2} \int d^3 r_{\mathrm{A}}\ \Theta_3^{\mathrm{A}} \int d^3 r_{\mathrm{B}}\ \Theta_1^{\mathrm{B}} \frac{r_{\mathrm{A}}^4 \omega_3(r_{\mathrm{A}})\omega_1(r_{\mathrm{B}})}{d_{3\mathrm{A}}^2 \omega_3(r_{\mathrm{A}}) + d_{1\mathrm{B}}^2 \omega_1(r_{\mathrm{B}})}$$
$$+ \frac{875 d_{2\mathrm{A}} d_{2\mathrm{B}}}{32\pi^2} \int d^3 r_{\mathrm{A}}\ \Theta_2^{\mathrm{A}} \int d^3 r_{\mathrm{B}}\ \Theta_2^{\mathrm{B}} \frac{r_{\mathrm{A}}^2 r_{\mathrm{B}}^2 \omega_2(r_{\mathrm{A}})\omega_2(r_{\mathrm{B}})}{d_{2\mathrm{A}}^2 \omega_2(r_{\mathrm{A}}) + d_{2\mathrm{B}}^2 \omega_2(r_{\mathrm{B}})}\,, \quad (43)$$

where $\Theta_l^{\mathrm{A}} = \Theta(R_l^{\mathrm{A}} - r_{\mathrm{A}})$ and the same for Θ_l^{B}. Similar to the evaluation of C_6 [see Eq. (15)], the numerical integrations required to evaluate Eqs. (42) and (43) are double integrations of the form:

$$\int_0^\infty dr_{\mathrm{A}} \int_0^\infty dr_{\mathrm{B}} f(r_{\mathrm{A}}, r_{\mathrm{B}})\,. \quad (44)$$

As a further test, we applied the above formulas to calculate C_8 and C_{10} for a large set of atom pairs, consisting of rare-gas atoms (He, Ne, Ar, Kr, Xe), hydrogen and alkali-metal atoms (H, Li, Na, K) and alkaline-earth atoms (Be, Mg, Ca). These atom pairs have been used to study C_6 (see Table 2). Here we choose them, because their static multipole polarizabilities are accurately known. They are tabulated in Table 1. The calculated higher-order coefficients are displayed in Tables 5 and 6. The MARE was calculated using the reference values obtained from highly-accurate many-body methods. The results show that the MARE for C_8 and C_{10} is nearly the same as that for C_6. In order to better understand the physics for higher-order coefficients, a comparison of the cutoff radii on the dipole, quadrupole and octupole polarizabilities has been made and displayed in Table 1. From Table 1 we observe that the cutoff radii are also close to each other for all three coefficients, and to conventionally-defined vdW radii $\alpha_1(0)^{1/3}$. This is expected, because all cutoff radii

Table 5. The vdW coefficients C_8 (in atomic units) calculated with spin-restricted Hartree–Fock densities.[69] The MARE is 3.0%.

	Reference	Present		Reference	Present
He–He	14.14[a]	13.57	Ar–H	442.1[b]	445.6
Ne–Ne	90.34[b]	98.73	Ar–Li	9493[h]	9394.4
Ar–Ar	1634[a]	1695	Ar–Na	11530[h]	10837
Kr–Kr	4187[b]	4112	Ar–K	22280[h]	21369
Xe–Xe	12807[b]	12443	Kr–H	732.3[b]	717.19
He–Ne	36.18[b]	37.06	Kr–Li	14760[h]	14603
He–Ar	167.5[b]	168.8	Kr–Na	17870[h]	16806
He–Kr	280.0[b]	274.1	Kr–K	34310[h]	32886
He–Xe	525.0[b]	511.0	Xe–H	1357[b]	1322
Ne–Ar	390.1[b]	416.6	Xe–Li	25210[h]	25373
Ne–Kr	638.1[b]	660.1	Xe–Na	30330[h]	29046
Ne–Xe	1162[b]	1193	Xe–K	57510[h]	56014
Ar–Kr	2617[b]	2650	He–Be	450.2[g]	428.3
Ar–Xe	4669[b]	4698	He–Mg	883.5[g]	873.8
Kr–Xe	7389[b]	7214	He–Ca	2139[i]	2213
H–H	124.4[c]	122.6	Ne–Be	899.5[g]	950.6
Li–Li	81830[d]	81315	Ne–Mg	1805[g]	1885
Na–Na	109000[d]	104546	Ne–Ca	4368[i]	4641
K–K	389200[d]	388071	Ar–Be	3850[g]	3932
H–Li	3280[e]	3195	Ar–Mg	7675[g]	7753
H–Na	3856[d]	3709	Ar–Ca	18150[i]	18932
H–K	7396[d]	7497	Kr–Be	5985[g]	6112
Li–Na	94850[d]	92739	Kr–Mg	11850[g]	11952
Li–K	185200[d]	183769	Kr–Ca	27910[i]	28922
Na–K	208200[d]	204322	Xe–Be	10380[g]	10689
Be–Be	10220[f]	10397	Xe–Mg	20250[g]	20560
Mg–Mg	41640[f]	40302	Xe–Ca	46750[i]	48823
Ca–Ca	226000[f]	226159	H–Be	1251[g]	1218
Be–Mg	20820[f]	20689	H–Mg	2575[g]	2517
Be–Ca	50070[f]	51238	H–Ca	6301[i]	6456
Mg–Ca	98070[f]	97279	Li–Be	27880[f]	27582
He–H	41.73[g]	41.02	Li–Mg	56830[f]	55417
He–Li	1084[f]	1052	Li–Ca	141300[f]	139856
He–Na	1328[f]	1219	Na–Be	33490[f]	31649
He–K	2623[f]	2467	Na–Mg	67360[f]	62733
Ne–H	97.82[b]	100.6	Na–Ca	163300[f]	154955
Ne–Li	2229[h]	2226	K–Be	65140[f]	62285
Ne–Na	2721[h]	2573	K–Mg	128300[f]	120908
Ne–K	5309[h]	5132	K–Ca	302400[f]	289105

[a]Ref. 75, [b]Ref. 74, [c]Ref. 77, [d]Ref. 34, [e]Ref. 95, [f]Ref. 79, 80, [g]Ref. 73, [h]Ref. 82, [i]Ref. 83.

Table 6. The vdW coefficients C_{10} (in atomic units) calculated with spin-restricted Hartree–Fock densities.[69] The MARE is 3.1%.

	Reference	Present		Reference	Present
He–He	185.8[a]	172.9	Ar–H	12617[b]	12805
Ne–Ne	1535.6[b]	1621.5	Ar–Li	678100[h]	678888
Ar–Ar	49380[a]	51302	Ar–Na	876900[h]	876616
Kr–Kr	152800[a]	154925	Ar–K	2132000[h]	2176341
Xe–Xe	619840[b]	612026	Kr–H	23441[b]	23328
He–Ne	545.08[b]	543.53	Kr–Li	1087000[h]	1085461
He–Ar	3701.1[b]	3726.1	Kr–Na	1398000[h]	1388046
He–Kr	7256.6[b]	7208.0	Kr–K	3352000[h]	3397544
He–Xe	16674[b]	16594	Xe–H	51088[b]	50783
Ne–Ar	9335.2[b]	9904.4	Xe–Li	1957000[h]	1985390
Ne–Kr	17658[b]	18402	Xe–Na	2490000[h]	2498750
Ne–Xe	38978[b]	40577	Xe–K	5836000[h]	5961000
Ar–Kr	88260[b]	90207	He–Be	14585[g]	16339
Ar–Xe	184250[b]	187801	He–Mg	39360[g]	43665
Kr–Xe	316030[b]	313588	He–Ca	131900[i]	137782
H–H	3285[c]	3262	Ne–Be	34800[g]	38397
Li–Li	7289000[d]	7240684	Ne–Mg	90500[g]	98501
Na–Na	11340000[e]	10540429	Ne–Ca	279800[i]	302361
K–K	53740000[e]	51032647	Ar–Be	176000[g]	177602
H–Li	223200[f]	219959	Ar–Mg	431000[g]	437099
H–Na	291600[f]	287570	Ar–Ca	1238000[i]	1305655
H–K	734400[f]	738040	Kr–Be	295000[g]	295752
Li–Na	8859000[d]	8784051	Kr–Mg	706000[g]	709140
Li–K	19490000[d]	20327353	Kr–Ca	1981000[i]	2078601
Na–K	23030000[d]	23791361	Xe–Be	584000[g]	576090
Be–Be	516500[e]	578184	Xe–Mg	1340000[g]	1328483
Mg–Mg	2817000[e]	3022005	Xe–Ca	3559000[i]	3776913
Ca–Ca	22000000[e]	22755416	H–Be	47400[g]	51228
Be–Mg	1232000[e]	1352866	H–Mg	122000[g]	133168
Be–Ca	3713000[e]	3917828	H–Ca	402400[i]	414861
Mg–Ca	8088000[e]	8426903	Li–Be	2066000[e]	2109778
He–H	865.85[g]	852.87	Li–Mg	4541000[e]	4610879
He–Li	72602[e]	71730	Li–Ca	12610000[e]	12651840
He–Na	95140[e]	95083	Na–Be	2651000[e]	2651037
He–K	239800[e]	245028	Na–Mg	5743000[e]	5665753
Ne–H	2220.5[b]	2283	Na–Ca	15610000[e]	15210198
Ne–Li	153100[h]	155631	K–Be	6382000[e]	6431770
Ne–Na	199300[h]	204268	K–Mg	13350000[e]	13212637
Ne–K	493600[h]	516208	K–Ca	34620000[e]	33995651

[a]Ref. 75, [b]Ref. 74, [c]Ref. 77, [d]Ref. 34, [e]Ref. 79, 80, [f]Ref. 95, [g]Ref. 73, [h]Ref. 82, [i]Ref. 83.

Table 7. Comparison of different models for the vdW coefficients C_8 and C_{10} (in atomic units) for atom pairs. SSM = solid-sphere model and BJ = Becke–Johnson and MARE = mean absolute relative error. The reference values are taken from Tables 5 and 6, and the solid-sphere values are taken from Ref. 61 (see Tables 5 and 6).

Atom pair	C_8^{ref}	SSM	BJ[a]	Lima[b]	C_{10}^{ref}	SSM	BJ[a]	Lima[b]
He–He	14.14	13.57	16.15	14.17	185.8	172.9	214.2	189.7
Ne–Ne	90.34	98.73	97.40	90.98	1536	1622	1625	1556
Ar–Ar	1634	1695	2082	1642	49380	51302	64960	50096
Kr–Kr	4187	4112	5287	3985	152800	154925	198379	151869
Xe–Xe	12807	12443	15922	11928	619840	612026	766727	594677
He–Ne	36.18	37.06	41.05	36.82	545.1	543.5	598.8	557.2
He–Ar	167.5	168.8	211.2	168.8	3701	3726	4475	3797
He–Kr	280.0	274.1	351.0	274.7	7257	7208	8499	7349
He–Xe	525.0	511.0	649.2	508.8	16674	16594	18896	16823
Ne–Ar	390.1	416.6	464.2	392.8	9335	9904	11050	9529
Ne–Kr	638.1	660.1	757.8	624.3	17658	18402	20399	17772
Ne–Xe	1162	1193	1370	1126	38978	40577	43819	39138
Ar–Kr	2617	2650	3329	2570	88260	90207	114390	88334
Ar–Xe	4669	4698	5869	4540	184250	187801	232344	183535
Kr–Xe	7389	7214	9234	6957	316030	313588	395106	306308
H–H	124.4	122.6	152.1	124.4	3285	3262	4438	3286
H–He	41.73	41.02	48.37		865.9	852.9	1065	
H–Ne	97.82	100.6	111.7		72602	71730	2619	
H–Ar	442.1	445.6	560.5		12617	12805	16496	
H–Kr	732.3	717.19	920.6		23441	23328	29671	
H–Xe	1357	1322	1688		51088	50783	62297	
MARE		3%	22%			3%	22%	

[a]Ref. 55, [b]Ref. 54.

equal the sphere radius R for a classical metallic sphere. The inhomogeneity and diffuse nature of the electron density slightly modifies the cutoff, but this modification is quite important. Nearly the same MARE and cutoff radius indicate that the physics behind the model dynamic dipole polarizability has been successfully transferred to the model dynamic multipole polarizabilities. It seems that the solid-sphere model may generate dynamic multipole polarizabilities and vdW coefficients to any desired order without losing accuracy, because the generalization does not rely on empirical fitting, but just the correct transfer of the physics from one order to another. Thus the solid-sphere model provides a nearly-correct account of the vdW interaction. For application of C_6, C_8 and C_{10}, see Refs. 22, 33 and 96.

Finally, we compare the higher-order coefficients C_8 and C_{10} with those obtained from the Becke–Johnson and Lima's models. From Table 7 we see that our nonempirical solid-sphere model can achieve comparable accuracy of Lima's empirical model, but it is much more accurate than Becke–Johnson.

In summary, we have formulated a unified theory for the dynamic multipole polarizabilities and vdW coefficients. Numerical tests on diverse atom pairs show that

the extension is very successful, because the accuracy for both the leading-order and higher-order coefficients is nearly the same. This remarkable feature allows us to treat the leading-order as well as higher-order coefficients on the same footing. Consistent accuracy is significantly important, because it guarantees that our model should also be able to describe other many-body vdW interactions (such as Axilrod–Teller–Muto three-body terms) as well. The required inputs are the true static multipole polarizability and the electron density. Since the static polarizability contains nearly all of the many-body effects and the geometry effect, the model dynamic multipole polarizability should be able to capture the nonsphericity of the electron density and can achieve remarkable accuracy. Since the input, the electronic density and the static polarizabilities, are accessible from the ground-state DFT,[97,98] we have in principle a true DFT approach for the dynamic multipole polarizabilities and vdW coefficients and therefore may save a significant amount of computer time.

5. Classical Model for the vdW Coefficients Between Nanostructures

The solid-sphere model can achieve remarkable accuracy for atoms and quasispherical systems, but it may be unsuitable to cage molecules with a concentric cavity such as fullerenes. Fullerenes can be modeled with a quasispherical shell of the electron density, within which the density is nearly uniform, due to the π-electron delocalization over the whole skeleton of fullerene molecules. Outside the shell, the density radially decays exponentially. Natural questions that one would like to ask are whether the solid-sphere model is able to describe cage molecules such as fullerenes and why. In this section, we will discuss a recent work, which successfully addressed these issues from the view of classical physics. While the classical model may not be accurate for atoms, small molecules and clusters, due to the rapid variation of the electron density, it can provide useful insights into the van der Waals interaction involving cage molecules in a simpler and easily understandable way. These insights are of particular value, considering the computational challenges with first-principles calculations for the vdW interactions between large systems.

Let us consider a classical conducting spherical shell of density with the outer radius R and shell thickness t. The electron density is uniform within the shell and zero outside the shell. For such a density, the exact expression for the dynamic multipole polarizability is given by[62,66,99]:

$$\alpha_l(iu,t) = \left[R^{2l+1}\frac{\epsilon-1}{\epsilon+(l+1)/l}\right]\frac{1-\rho_l}{1-\beta_l\rho_l}\,, \tag{45}$$

$$\beta_l = \frac{(\epsilon-1)^2}{[\epsilon+l/(l+1)][\epsilon+(l+1)/l]}\,, \tag{46}$$

$$\rho_l = \left(\frac{R-t}{R}\right)^{2l+1}. \tag{47}$$

In the long wavelength limit, the dielectric function of the isotropic media is

$$\epsilon(iu) = 1 + \omega_p^2/u^2 \,. \tag{48}$$

Substituting Eq. (48) into Eqs. (45) and (46) leads to a simple expression[62,99]

$$\alpha_l(iu) = \left(R^{2l+1} \frac{\omega_l^2}{\omega_l^2 + u^2} \right) \frac{1 - \rho_l}{1 - \beta_l \rho_l} \,, \tag{49}$$

$$\beta_l = \frac{\omega_l^2 \ \tilde{\omega}_l^2}{(\omega_l^2 + u^2)(\tilde{\omega}_l^2 + u^2)} \,, \tag{50}$$

where $\omega_l = \omega_p \sqrt{l/(2l+1)}$ is the mode vibrational frequency of the spherical shell and $\tilde{\omega}_l = \omega_p \sqrt{(l+1)/(2l+1)}$ is the mode vibrational frequency of cavity. The quantity in parentheses of Eq. (49) is the dynamic multipole polarizability of a classical metallic solid sphere, while the remaining part, which is also frequency-dependent, is due to the cavity. When the cavity vanishes (i.e., $t = R$), the dynamic multipole polarizability of the classical conducting spherical shell reduces to that of a classical conducting solid sphere. From the classical model, we see that the cavity may affect the dynamical multipole polarizability via two ways: Electron density distribution and frequency dependence. The second effect of the cavity described with β_l arises from a coupling between the sphere and cavity plasmon vibrations. The second effect can be significantly important. We may attribute the failure of the solid-sphere model and other previous methods for cage molecules to the omission of this effect.

In the static limit, we immediately have

$$\alpha_l(0) = R^{2l+1} \,. \tag{51}$$

Since the outer radius of the shell is fixed for a classical conducting spherical shell, this relationship may provide a useful estimate of static higher-order multipole polarizability from the static dipole polarizability. This estimate may be crude for small systems, but it should be reasonable for large systems, in particular when the size of a system approaches the bulk limit, where the electron density is slowly varying. Another input is t, the thickness of the shell, which is defined by[100]:

$$R = R_n + t/2 \,, \tag{52}$$

where R_n is the average radius of the nuclear framework which can be calculated accurately[100,101] from molecular dynamics and DFT methods. The plasmon frequency of the extended uniform electron gas $\omega_p = \sqrt{4\pi\bar{n}}$ is calculated from the average electron density $\bar{n}$ of the shell. It is defined by

$$n = N/V, \quad V = (4\pi/3)R^3 - (4\pi/3)(R-t)^3 \,, \tag{53}$$

where N is the number of valence electrons and V is the volume of the shell.

The vdW coefficients within the classical model can be obtained by substituting Eq. (49) into Eq. (3). The result is:

$$C_{2k}^{\mathrm{AB}} = \frac{(2k-2)!}{32\pi^3} \sum_{l_1=1}^{k-2} \frac{(2l_1+1)(2l_2+1)}{(2l_1)!(2l_2)!} \frac{1}{d_{l_1}^{\mathrm{A}} d_{l_2}^{\mathrm{B}}} \int_{R_{l_1}^{\mathrm{A}}-t_{l_1}^{\mathrm{A}}}^{R_{l_1}^{\mathrm{A}}} d^3 r_{\mathrm{A}}\ r_{\mathrm{A}}^{2l_1-2} [(d_{l_1}^{\mathrm{A}})^2 \omega_{l_1}^{\mathrm{A}}]^2$$

$$\times \int_{R_{l_2}^{\mathrm{B}}-t_{l_2}^{\mathrm{B}}}^{R_{l_2}^{\mathrm{B}}} d^3 r_{\mathrm{B}}\ r_{\mathrm{B}}^{2l_2-2} [(d_{l_2}^{\mathrm{B}})^2 \omega_{l_2}^{\mathrm{B}}]^2 I_{l_1 l_2}^{\mathrm{AB}}, \tag{54}$$

$$I_{l_1,l_2}^{\mathrm{AB}} = \frac{\pi}{2Q_{l_1 l_2}^{\mathrm{AB}}} \sum_{i=1}^{3} \left[f_i(a_{l_1}^{\mathrm{A}}, a_{l_2}^{\mathrm{B}}; b_{l_1}^{\mathrm{A}}, b_{l_2}^{\mathrm{B}}) / D(a_{l_1}^{\mathrm{A}}, a_{l_2}^{\mathrm{B}}) + f_i(b_{l_1}^{\mathrm{A}}, b_{l_2}^{\mathrm{B}}; a_{l_1}^{\mathrm{A}}, a_{l_2}^{\mathrm{B}}) / D(b_{l_1}^{\mathrm{A}}, b_{l_2}^{\mathrm{B}}) \right], \tag{55}$$

where

$$Q_{l_1 l_2}^{\mathrm{AB}} = [(a_{l_1}^{\mathrm{A}})^2 - (b_{l_1}^{\mathrm{A}})^2][(a_{l_1}^{\mathrm{A}})^2 - (b_{l_2}^{\mathrm{B}})^2][(a_{l_2}^{\mathrm{B}})^2 - (b_{l_1}^{\mathrm{A}})^2][(a_{l_2}^{\mathrm{B}})^2 - (b_{l_2}^{\mathrm{B}})^2], \tag{56}$$

$$D(x,y) = xy(x+y)\,, \tag{57}$$

$$a_l = \frac{d_l^2\sqrt{2}}{2} \left[(\omega_l^2 + \tilde{\omega}_l^2) - \sqrt{(\omega_l^2 - \tilde{\omega}_l^2)^2 + 4\rho_l \omega_l^2 \tilde{\omega}_l^2} \right]^{1/2}, \tag{58}$$

$$b_l = \frac{d_l^2\sqrt{2}}{2} \left[(\omega_l^2 + \tilde{\omega}_l^2) + \sqrt{(\omega_l^2 - \tilde{\omega}_l^2)^2 + 4\rho_l \omega_l^2 \tilde{\omega}_l^2} \right]^{1/2}, \tag{59}$$

$$f_1(p,q;s,t) = (pq)^4 + (pq)^3(s^2+t^2) - pq(st)^2(p^2+pq+q^2), \tag{60}$$

$$f_2(p,q;s,t) = -\{[(d_{l_1}^{\mathrm{A}})^2 \tilde{\omega}_{l_1}^{\mathrm{A}}]^2 + [(d_{l_2}^{\mathrm{B}})^2 \tilde{\omega}_{l_2}^{\mathrm{B}}]^2\}$$
$$\times [(pq)^2(p^2+pq+q^2-s^2-t^2) - pq(st)^2]\,, \tag{61}$$

$$f_3(p,q;s,t) = [(d_{l_1}^{\mathrm{A}})^2 \tilde{\omega}_{l_1}^{\mathrm{A}}]^2 [(d_{l_2}^{\mathrm{B}})^2 \tilde{\omega}_{l_2}^{\mathrm{B}}]^2 [p^4 + p^3 q + p^2 q^2 + pq^3 + q^4$$
$$- (p^2+pq+q^2)(s^2+t^2) + (st)^2]\,. \tag{62}$$

Note that the vdW coefficients are symmetric with respect to the exchange of A and B.

The classical model is valid for any value of t. Thus it is applicable not only to fullerenes, but also to clusters with no cavity. This advantage allows us to study the vdW interaction for any molecular pair of quasispherical symmetry on the same footing, regardless whether a system has a cavity or not. Our recent work shows that the model is quite accurate for sodium–sodium and sodium–fullerene clusters, with a mean absolute relative deviation of about 7% from TDDFT or TD Hartree–Fock methods.

The classical model is suitable to nanosize or larger systems, in particular when the size of systems approaches their bulk limit, because in that limit, the typical electron density is slowly-varying. This model has been employed to study the

asymptotic size dependence of the coefficients for a few families of cluster pairs, including fullerene pairs. For convenience, we denote the number of atoms in the cluster as n (a symbol we used earlier for the density). Since the electron density approaches a constant in the bulk limit, we have in the asymptotic region

$$n \sim R^{\delta}\,, \tag{63}$$

where δ is the dimensionality of a cluster. $\delta = 3$ for solid clusters, in which the atoms are distributed over the three-dimensional space and 2 for fullerenes, where the atoms are distributed over the two-dimensional surface. For a solid sphere, $t = R$. Then from Eqs. (3) and (45), we obtain the size dependence of the vdW coefficients for identical cluster pairs,

$$C_{2k}^{AA} \sim R^{2k} \sim n^{2k/\delta}, \quad (\delta = 3)\,. \tag{64}$$

According to the atom pairwise interaction picture, the number of ways to pair an atom in a piece of density with one in another piece is n^2. This size dependence is consistent with the above analysis for C_6^{AA}. For C_8^{AA} and C_{10}^{AA}, the classical theory predicts $C_8^{AA} \sim n^{8/3}$ and $C_{10}^{AA} \sim n^{10/3}$. The size dependence of C_8^{AA} in the atom pairwise interaction picture has a correction term arising from C_6, due to the distance adjustment of each atom pair, while the size dependence of C_{10}^{AA} in this picture has two correction terms, one of which arises from C_6 and the other from C_8, due to the distance adjustment of each atom pair.

For cage molecules with a cavity such as fullerenes, it was shown[62] that in the asymptotic region (i.e., $n \to \infty$),

$$C_{2k}^{AA} \sim R^{2k}(t/R)^2/(t/R)^{3/2} \sim R^{2k-1/2} \sim n^{(2k-1/2)/\delta}\,, \tag{65}$$

where $\delta = 2$. Thus for a pair of identical fullerenes, $C_6^{AA} \sim n^{2.75}$, which clearly exhibits a stronger size dependence than that for a solid clusters such as sodium and silicon clusters.

We calculated the asymptotic behavior of the vdW coefficients for fullerene, sodium and silicon clusters. The inputted static dipole polarizabilities of sodium and silicon clusters are given in Table 8. While the static dipole polarizabilities of fullerenes calculated with the tight binding method are available in the literature,[100] we find that these literature values were overestimated, because the thickness t evaluated from Eq. (52) increases too rapidly with fullerene size. Because the average radius of the nuclear framework for fullerenes is much more easily calculated[100,101] with molecular dynamics and DFT and because the thickness t has a very weak dependence upon the size of fullerenes, we estimated the static dipole polarizability of fullerenes from the relationship of Eq. (52) using a fixed thickness value $t = 2.77$ for C_{60}. In Table 8, only the average radius of the nuclear framework is listed. All the higher-order static polarizabilities of these clusters were estimated from the classical relationship (51).

From Tables 9–12, we can observe that the vdW coefficients for cluster pairs display an asymptotic tendency, as predicted by Eqs. (64) and (65).

Table 8. Static dipole polarizabilities (in Hartree atomic units) of sodium and silicon clusters, and the average radii of the nuclear framework of fullerenes.

Na_n	$\alpha_1(0)$	Fullerene	R_n	Si_n	$\alpha_1(0)$
Na_2	259.5[a]	C_{20}	3.93[c]	Si_9	266[e]
Na_4	511.5[a]	C_{60}	6.73[c]	Si_{10}	291[e]
Na_6	743.9[a]	C_{240}	13.08[c]	Si_{11}	317[e]
Na_8	883.9[a]	C_{540}	19.50[c]	Si_{12}	359[e]
Na_{10}	1053[a]	C_{960}	25.53[c]	Si_{13}	393[e]
Na_{12}	1342[a]	C_{2160}	38.74[c]	Si_{20}	619[f]
Na_{14}	1652[a]	C_{3840}	50.57[c]	Si_{21}	663[f]
Na_{18}	1725[a]			Si_{22}	674[f]
Na_{20}	1988[a]	Si_n	$\alpha_1(0)$	Si_{23}	700[f]
Na_{40}	3498[b]	Si_3	108[d]	Si_{24}	737[f]
Na_{58}	4899[b]	Si_4	138[d]	Si_{25}	776[f]
Na_{92}	7481[b]	Si_5	164[d]	Si_{26}	825[f]
		Si_6	179[d]	Si_{27}	845[f]
		Si_7	214[d]	Si_{28}	863[f]
		Si_8	250[e]		

[a]Ref. 102, [b]Ref. 103 [c]Ref. 104, [d]Ref. 105, [e]Ref. 106, [f]Ref. 107.

Table 9. Model radius $R = \alpha_1(0)^{1/3}$ and van der Waals coefficients (in hartree atomic units) for Na_n-Na_n , demonstrating the predicted asymptotic behavior of Eq. (64). One valence electron per atom. The reference value for $\alpha_1(0)$ and the coefficients C_6, C_8, and C_{10} are taken from Refs. 62 and 15, respectively.

n	R	$\frac{C_6}{10^3 n^2}$	$\frac{C_8}{10^5 n^{8/3}}$	$\frac{C_{10}}{10^7 n^{10/3}}$
2	6.38	1.11	1.49	1.65
4	8.00	1.08	1.44	1.59
6	9.06	1.04	1.34	1.45
8	9.60	0.87	1.05	1.05
10	10.17	0.81	0.95	0.91
12	11.03	0.89	1.08	1.08
14	11.82	0.96	1.21	1.26
18	11.99	0.70	0.77	0.70
20	12.57	0.74	0.83	0.78
40	15.18	0.61	0.63	0.54
58	16.98	0.58	0.59	0.49
92	19.56	0.55	0.54	0.44

Table 10. Model outer radius $R = \alpha_1(0)^{1/3}$, shell thickness $t = 2(R - R_n)$ and vdW coefficients for fullerene pairs C_n-C_n, in hartree atomic units, demonstrating the predicted asymptotic behavior of Eq. (64). Four valence electrons per atom. From $n = 20$–3840, C_6 increases by a factor of more than 394,000 and C_{10} by more than 5.5×10^9. Note that the asymptotic limit ($n \to \infty$) is reached slowly when t/R differs from 1. Note that the larger fullerences may be nonspherical (e.g., icosahedral in C_{540}), but this should not affect our conclusion.

n	R	t	$C_6/n^{11/4}$	$C_8/(10n^{15/4})$	$C_{10}/(100n^{19/4})$
20	5.13	2.40	2.75	1.98	1.14
60	8.11	2.76	1.75	1.07	0.53
240	14.46	2.76	1.00	0.37	0.20
540	20.88	2.76	0.82	0.23	0.14
960	26.91	2.76	0.70	0.16	0.11
2160	40.12	2.76	0.67	0.11	0.10
3840	51.95	2.76	0.57	0.08	0.09

Table 11. Model radius $R = \alpha_1(0)^{1/3}$ and vdW coefficients for Si_n-Si_n, in hartree atomic units, demonstrating the predicted asymptotic behavior of Eq. (64). Four valence electrons per atom.

n	R	$C_6/10^3n^2$	$C_8/10^5n^{8/3}$	$C_{10}/10^7n^{10/3}$
3	4.76	0.324	0.185	0.087
4	5.17	0.304	0.168	0.078
5	5.47	0.282	0.151	0.067
6	5.63	0.244	0.123	0.051
7	5.98	0.254	0.130	0.055
8	6.30	0.262	0.136	0.059
9	6.43	0.241	0.120	0.050
10	6.63	0.235	0.117	0.048
11	6.82	0.232	0.114	0.047
12	7.11	0.245	0.124	0.052
13	7.32	0.249	0.126	0.053
20	8.52	0.258	0.133	0.057
21	8.72	0.266	0.139	0.060
22	8.77	0.254	0.130	0.055
23	8.88	0.252	0.128	0.054
24	9.03	0.255	0.131	0.056
25	9.19	0.259	0.134	0.057

6. Conclusion and Outlook

Many-electron wavefunction methods can predict accurate dynamic multipole polarizabilities and vdW coefficients C_{2k} for small objects, but are impractical for large nanostructures, where density-functional-like methods are more feasible. Even TDDFT and TD Hartree–Fock methods are too computationally costly for large systems. Explicit density functional approximations or models for the polarizabilities and vdW coefficients are thus needed.

Table 12. Calculated vdW coefficients for Na_n–C_{60}, in hartree atomic units. Note that the asymptotic ($n \to \infty$) limit is reached more slowly when B $\neq$ A.

n	$C_6/10^3n^2$	$C_8/10^5n^{8/3}$	$C_{10}/n^{10/3}$
2	8.04	14.06	20.43
4	7.92	10.79	12.11
6	7.80	9.25	9.04
8	7.32	7.65	6.58
10	7.14	6.89	5.46
12	7.20	7.01	5.42
14	7.62	7.16	5.45
18	6.78	5.49	3.60
20	6.90	5.58	3.63
40	6.42	4.34	2.31
58	6.30	3.98	1.96
92	6.12	3.63	1.64

Efficient and accurate calculation of vdW energy is a hot topic and plays an important role in electronic structure calculations. Considerable progress toward understanding of this quantity at a fundamental level has been made. Some methods[55,56,58,61] have achieved excellent accuracy for free atom pairs, without relying on the adjustment of empirical parameters. In this review, we limit our discussion to atom pairs. Some interesting works by Scheffler's group[57,60] and by Dobson and his collaborators[63] have not been discussed in detail in this paper, although these methods have shown their promise in practical applications.[25,26]

Acknowledgments

This work was supported by two NSF grants: NSF Cooperative Agreement No. EPS-1003897 with additional support from the Louisiana Board of Regents and Grant No. DMR-0854769.

References

1. T. L. Barr and E. R. Davidson, *Phys. Rev. A* **1**, 644 (1970).
2. I. N. Levine, *Quantum Chemistry*, 6th edn. (Pearson Education Ltd, London, 2000).
3. I. Shavitt and R. J. Bartlett, *Many-Body Methods in Chemistry and Physics: MBPT and Coupled-Cluster Theory* (Cambridge University Press, Cambridge, 2009).
4. R. J. Bartlett and M. Musiał, *Rev. Mod. Phys.* **79**, 291 (2007).
5. W. M. C. Foulkes, L. Mitas, R. J. Needs and G. Rajagopal, *Rev. Mod. Phys.* **73**, 33 (2001).
6. R. G. Parr and W. Yang, *Density Functional Theory of Atoms and Molecules* (Oxford University Press, Oxford, 1989).
7. K. D. Sen (ed.), *Reviews in Modern Quantum Chemistry: A Celebration of the Contributions of R. G. Parr* (World Scientific, Singapore, 2002).

8. W. Kohn and L. J. Sham, *Phys. Rev.* **140**, A1133 (1965).
9. C. Fiolhais, F. Nogueira and M. Marques (eds.), *A Primer in Density Functional Theory*, Lecture Notes in Physics, Vol. 620 (Springer, Berlin, 2003).
10. S. H. Vosko, L. Wilk and M. Nusair, *Can. J. Phys.* **58**, 1200 (1980).
11. J. P. Perdew and Y. Wang, *Phys. Rev. B* **45**, 13244 (1992).
12. A. Becke, *Phys. Rev. A* **38**, 3098 (1988).
13. C. Lee, W. Yang and R. G. Parr, *Phys. Rev. B* **37**, 785 (1988).
14. A. D. Becke, *J. Chem. Phys.* **104**, 1040 (1996).
15. J. P. Perdew, in *Electronic Structure of Solids*, P. Ziesche and H. Eschrig (eds.) (Akademie Verlag, Berlin, 1991), p. 11.
16. J. P. Perdew, K. Burke and M. Ernzerhof, *Phys. Rev. Lett.* **77**, 3865 (1996).
17. J. Tao, J. P. Perdew, V. N. Staroverov and G. E. Scuseria, *Phys. Rev. Lett.* **91**, 146401 (2003).
18. Y. Zhao and D. G. Truhlar, *J. Chem. Phys.* **125**, 194101 (2006).
19. J. Heyd, G. E. Scuseria and M. Ernzerhof, *J. Chem. Phys.* **118**, 8207 (2003).
20. J. Tao and J. P. Perdew, *J. Chem. Phys.* **122**, 114102 (2005).
21. G. I. Csonka, J. P. Perdew, A. Ruzsinszky, P. H. T. Philipsen, S. Lebégue, J. Paier, O. A. Vydrov and J. G. Angyán, *Phys. Rev. B* **79**, 155107 (2009).
22. L. Goerigk and S. Grimme, *Phys. Chem. Chem. Phys.* **13**, 6670 (2011).
23. S. Grimme, J. Antony, S. Ehrlich and H. J. Krieg, *Chem. Phys.* **132**, 154104 (2010).
24. S. Grimme, *Comput. Mol. Sci.* **1**, 211 (2011).
25. B. Santra, J. Klimeš, D. Alfè, A. Tkatchenko, B. Slater, A. Michaelides, R. Car and M. Scheffler, *Phys. Rev. Lett.* **107**, 185701 (2011).
26. G.-X. Zhang, A. Tkatchenko, J. Paier, H. Appel and M. Scheffler, *Phys. Rev. Lett.* **107**, 245501 (2011).
27. Y. Fang *et al.*, *Phys. Rev. B* **87**, 214101 (2013).
28. Y. Andersson, E. Hult, P. Apell, D. C. Langreth and B. I. Lundqvist, *Solid State Commun.* **106**, 235 (1998).
29. E. Hult, P. Hyldgaard, J. Rossmeisl and B. I. Lundqvist, *Phys. Rev. B* **64**, 195414 (2001).
30. J. F. Dobson, A. White and A. Rubio, *Phys. Rev. Lett.* **96**, 073201 (2006).
31. K. T. Tang and J. P. Toennies, *J. Chem. Phys.* **80**, 3726 (1983).
32. Q. Wu and W. Yang, *J. Chem. Phys.* **116**, 515 (2002).
33. S. Grimme, S. Ehrlich and L. Goerigk, *J. Comput. Chem.* **32**, 1456 (2011).
34. S. H. Patil and K. T. Tang, *J. Chem. Phys.* **106**, 2298 (1997).
35. D. Spelsberg, T. Lorenz and W. Meyer, *J. Chem. Phys.* **99**, 7845 (1993).
36. K. T. Tang, J. M. Norbeck and P. R. Certain, *J. Chem. Phys.* **64**, 3063 (1976).
37. E. Zaremba and W. Kohn, *Phys. Rev. B* **13**, 2270 (1976).
38. V. P. Osinga, S. J. A. van Gisbergen, J. G. Snijders and E. J. Baerends, *J. Chem. Phys.* **106**, 5091 (2007).
39. E. Runge and E. K. U. Gross, *Phys. Rev. Lett.* **52**, 997 (1984).
40. S. J. A. van Gisbergen, J. G. Snijders and E. J. Baerends, *J. Chem. Phys.* **103**, 9347 (1995).
41. G. Vignale and W. Kohn, *Phys. Rev. Lett.* **77**, 2037 (1996).
42. J. Tao and G. Vignale, *Phys. Rev. Lett.* **97**, 036403 (2006).
43. A. Zangwill and P. Soven, *Phys. Rev. Lett.* **45**, 204 (1980).
44. A. Zangwill and P. Soven, *Phys. Rev. A* **21**, 1561 (1980).
45. A. Banerjee, A. Chakrabarti and T. K. Ghanty, *J. Chem. Phys.* **127**, 134103 (2007).
46. M. A. L. Marques, A. Castro, G. Malloci, G. Mulas and S. Botti, *J. Chem. Phys.* **127**, 014107 (2007).

47. V. A. Parsegian, *Van Der Waals Forces* (Cambridge University Press, Cambridge, 2005).
48. H. C. Hamaker, *Physica* **4**, 1058 (1937).
49. K. Rapcewicz and N. W. Ashcroft, *Phys. Rev. B* **44**, 4032 (1981).
50. Y. Andersson, D. C. Langreth and B. I. Lundqvist, *Phys. Rev. Lett.* **76**, 102 (1996).
51. J. F. Dobson and B. P. Dinte, *Phys. Rev. Lett.* **76**, 1780 (1996).
52. S. Grimme, *J. Comp. Chem.* **25**, 1463 (2004).
53. N. A. Lima and M. J. Caldas, *Phys. Rev. B* **72**, 033109 (2005).
54. N. A. Lima, *J. Chem. Phys.* **132**, 014110 (2010).
55. A. D. Becke and E. R. Johnson, *J. Chem. Phys.* **127**, 154108 (2007).
56. A. D. Becke and E. R. Johnson, *J. Chem. Phys.* **127**, 124108 (2007).
57. A. Tkatchenko and M. Scheffler, *Phys. Rev. Lett.* **102**, 073005 (2009).
58. J. Tao, J. P. Perdew and A. Ruzsinszky, *Phys. Rev. B* **81**, 233102 (2010).
59. O. A. Vydrov and T. Van Voorhis, *Phys. Rev. A* **81**, 062708 (2010).
60. A. Tkatchenko, R. A. DiStasio, R. Car and M. Scheffler, *Phys. Rev. Lett.* **108**, 236402 (2012).
61. J. Tao, J. P. Perdew and A. Ruzsinszky, *PNAS* **109**, 18 (2012).
62. A. Ruzsinszky, J. P. Perdew, J. Tao, G. I. Csonka and J. M. Pitarke, *Phys. Rev. Lett.* **109**, 233203 (2012).
63. J. F. Dobson and T. Gould, *J. Phys.: Condens. Matter* **24**, 073201 (2012).
64. J. P. Perdew, A. Ruzsinszky, J. Sun, S. Glindmeyer and G. I. Csonka, *Phys. Rev. A* **86**, 062714 (2012).
65. R. E. Goldstein, A. Parola and A. P. Smith, *J. Chem. Phys.* **91**, 1843 (1989).
66. A. A. Lucas, L. Henrard and P. Lambin, *Phys. Rev. B* **49**, 2888 (1994).
67. H. Margenau and N. R. Kestner, *Theory of Interatomic Forces*, 2nd edn. (Pergamon Press, Oxford, 1969).
68. D. M. Bishop and J. Pipin, *J. Chem. Phys.* **97**, 3375 (1992).
69. E. Clementi and C. Roetti, *At. Data Nucl. Data Tables* **14**, 177 (1974).
70. A. Z. Tang and F. T. Chan, *Phys. Rev. A* **33**, 3671 (1986).
71. P. Schwerdtfeger, Atomic static dipole polarizabilities, in *Atoms, Molecules and Clusters in Electric Fields. Theoretical Approaches to the Calculation of Electric Polarizability*, G. Maroulis (ed.), Vol. 1 (World Scientific, London, 2006), pp. 1–32.
72. A. Derevianko, W. R. Johnson, M. S. Safronova and I. F. Babb, *Phys. Rev. Lett.* **82**, 3589 (1999).
73. G. Figari, G. F. Musso and V. Magnasco, *Mol. Phys.* **50**, 1173 (1983).
74. A. J. Thakkar, H. Hettema and P. E. S. Wormer, *J. Chem. Phys.* **97**, 3252 (1992).
75. D. Spelsberg and W. Meyer, *J. Phys. Chem.* **100**, 14637 (1996).
76. M. Marinescu, H. R. Sadeghpour and A. Dalgarno, *Phys. Rev. A* **49**, 982 (1994).
77. A. Dalgarno and G. A. Victor, *Proc. Phys. Soc.* **90**, 605 (1967).
78. J. Mitroy and M. W. J. Bromley, *Phys. Rev. A* **68**, 062710 (2003).
79. J. Mitroy and M. W. J. Bromley, *Phys. Rev. A* **68**, 052714 (2003).
80. J. Mitroy and M. W. J. Bromley, *Phys. Rev. A* **71**, 019902 (2005) [Erratum: Phys. Rev. A **68**, 052714 (2003)].
81. F. Maeder and W. Kutzelnigg, *Chem. Phys.* **42**, 95 (1979).
82. J. Mitroy and J.-Y. Zhang, *Phys. Rev. A* **76**, 032706 (2007).
83. J. Mitroy and J.-Y. Zhang, *J. Chem. Phys.* **128**, 134305 (2008).
84. J. J. Rehr, E. Zaremba and W. Kohn, *Phys. Rev. B* **12**, 2062 (1975).
85. R. M. Nieminen and M. J. Puska, *Physica Scripta* **25**, 952 (1982).
86. G. D. Mahan, *J. Chem. Phys.* **76**, 493 (1981).
87. Z. H. Levine and S. G. Louie, *Phys. Rev. B* **25**, 6310 (1982).

88. K. L. Kelly, E. Coronado, L. L. Zhao and G. C. Schatz, *J. Phys. Chem. B* **107**, 668 (2003).
89. T. L. Ferrell and P. M. Echenique, *Phys. Rev. Lett.* **55**, 1526 (1985).
90. J. M. Pitarke, V. M. Silkin, E. V. Chulkov and P. M. Echenique, *Rep. Prog. Phys.* **70**, 1 (2007).
91. D. C. Langreth and M. J. Mehl, *Phys. Rev. B* **28**, 1809 (1983).
92. J. P. Perdew and Y. Wang, *Phys. Rev. B* **33**, 8800 (1986).
93. J. P. Perdew, K. Burke and Y. Wang, *Phys. Rev. B* **54**, 16533 (1996).
94. J. P. Perdew, A. Ruzsinszky, G. I. Csonka, L. A. Constantin and J. Sun, *Phys. Rev. Lett.* **103**, 026403 (2009).
95. J.-Y. Zhang and J. Mitroy, *Phys. Rev. A* **76**, 022705 (2007).
96. S. N. Steinmann, G. Csonka and C. Corminboeuf, *J. Chem. Theor. Comput.* **5**, 2950 (2009).
97. H. Sekino, Y. Maeda, M. Kamiya and K. Hirao, *J. Chem. Phys.* **126**, 014107 (2007).
98. T. M. Henderson, A. F. Izmaylov, G. Scalmani and G. E. Scuseria, *J. Chem. Phys.* **131**, 044108 (2009).
99. J. P. Perdew, J. Tao, P. Hao, A. Ruzsinszky, G. I. Csonka and J. M. Pitarke, *J. Phys.: Condens. Matter* **24**, 424207 (2012).
100. G. K. Gueorguiev, J. M. Pacheco and D. Tománek, *Phys. Rev. Lett.* **92**, 215501 (2004).
101. G. B. Adams, M. O'Keeffe and R. S. Ruoff, *J. Phys. Chem.* **98**, 9465 (1994).
102. A. Jiemchooroj, P. Norman and B. E. Sernelius, *J. Chem. Phys.* **125**, 124306 (2006).
103. D. E. Beck, *Phys. Rev. B* **30**, 6935 (1984).
104. G. K. Gueorguiev, J. M. Pacheco and D. Tománek, *Phys. Rev. Lett.* **92**, 215501 (2004).
105. G. Maroulis, D. Begué and C. Pouchan, *J. Chem. Phys.* **119**, 794 (2003).
106. V. E. Bazterra, M. C. Caputo and M. B. Ferraro, *J. Chem. Phys.* **117**, 11158 (2002).
107. K. A. Jackson, M. Yang, I. Chaudhuri and T. Frauenheim, *Phys. Rev. A* **71**, 033205 (2005).